

# Towards real-time optical measurement of microbubble content in hydrodynamic test facilities

<sup>1</sup>Patrick S. Russell\*; <sup>1</sup>Dean R. Giosio; <sup>1</sup>James A. Venning; <sup>1</sup>Bryce W. Pearce; <sup>1</sup>Paul A. Brandner  
V. Aumelas<sup>2</sup> and G. Maj<sup>2</sup>

<sup>1</sup>*Cavitation Research Laboratory, University of Tasmania, Launceston, Tasmania, Australia*

<sup>2</sup>*YLEC Consultants, Grenoble, France*

## Abstract

Real-time measurement of microbubble concentrations is desirable in order to inform experimental results, particularly in studies of cavitation physics. To develop these capabilities a controlled experiment using a micro-fluidic T-junction to produce mono-disperse microbubbles was devised with the size and frequency of microbubbles measured using a line-scan camera capable of acquiring 45k images per second. Measurements were able to be obtained and reported in under 3 seconds from the triggering time. Tests were carried out in quiescent water and implementation in non-stationary environments would extend the operational range. The principal operating mode produced microbubbles on the order of 80 to 130  $\mu\text{m}$  in size at frequencies ranging from 750 to 3200 bubbles per second across the range of air and water pressures tested.

**Keywords:** microbubbles; cavitation

## Introduction

Even small concentrations of microbubbles present within a fluid can greatly impact upon its mechanical properties. In particular the inception of cavitation inside facilities and on board vessels is often controlled by the largest microbubble which will pass through a region of low pressure. Consequently, real-time measurement of these concentrations is desirable in order to inform predicted performance and experimental results.

In hydrodynamic flows of practical interest cavitation nucleation is invariably heterogeneous where microbubbles entrained in the flow or ejected from surface hydrophobic crevices provide sites of weakness, or nuclei, for the initiation of phase change from liquid to vapour [1, 2]. The equilibrium of a microbubble becomes unstable below a critical pressure, depending on its diameter, after which it will grow explosively. Once activated bubbles fill with vapour and interact with the surrounding stationary or flowing liquid developing into macroscopic cavitation phenomena. Rigorous experimental modelling of the inception and dynamics of hydrodynamic cavitation in water tunnels thus requires control and measurement of the microbubble population. The variable pressure water (cavitation) tunnel within the Cavitation Research Laboratory (CRL) at the Australian Maritime College has been developed with ancillary systems for continuous artificial seeding and removal of microbubbles to provide controlled nuclei populations in the test flow [3, 4]. To date this capability has been developed using direct or dilute injection of poly-disperse microbubble populations generated through the rapid de-pressurisation and cavitation of supersaturated water [5]. Whilst poly-disperse populations (typically 10 to 100  $\mu\text{m}$  in diameter) are always required to model real flows the use of mono-disperse nuclei provides several advantages for basic research and for comparative experimental and computational work.

Microfluidic or lab-on-chip devices have been developed for mono-disperse generation of micro, or nano-bubble populations for sono-fluidic or sono-chemical processes such as contrast agents or drug delivery vectors in medical applications [6]. These devices typically generate smaller bubbles than those suitable for nuclei and may involve the use of surfactants [7]. Commercial devices using common materials and simple experimental set-ups generating microbubbles of order 10 to 100  $\mu\text{m}$  at rates of order  $10^3$  to  $10^4$  have been developed by YLEC Consultants, France. The present work is a collaboration between the CRL and YLEC Consultants to investigate the operational range and use of these devices for mono-disperse cavitation nuclei seeding.

\*Corresponding Author, Patrick Russell: [Patrick.Russell@utas.edu.au](mailto:Patrick.Russell@utas.edu.au)

To characterise such devices, or measure populations within the CRL hydrodynamic test facility long range microscopy-shadowgraphy is typically used. With the use of PIV cameras and dual pulse lasers bubble velocities may also be measured. However, the processing of these high resolution image pairs is demanding such that results can not, at present, be obtained in real-time. To address this problem a line-scan camera with a single row of densely spaced pixels was used. The reduced number of pixels allowed the acquisition speed of the camera to be high and the spatial resolution to be increased from standard PIV cameras in one dimension at the sacrifice of the second spatial dimension. When stacked these line measurements produce a space-time plot from which size and frequency information is readily extracted.

### Experimental overview

The L10 device from Ylec Consultants was mounted within a quiescent tank at atmospheric pressure and supplied by independently pressurised air and water lines. The size and frequency of bubbles produced was dependent on the balance of these pressures. The device was deemed to be in its principal operating mode when the standard deviation of the bubble size was 10% of the measured mean, with a single production frequency.

The T-junction device was tested in a 0.05 m square acrylic tank filled with distilled water. The junction was fitted through the base of the tank on a mount to which was connected the 4 mm pressurised air and water supply lines. Air pressure was regulated then conditioned through a 1.0  $\mu\text{m}$  filter before it reached the device. Water was supplied from a reservoir of distilled water pressurised by air connected to a second regulator. Water and air pressures ranging between 1.5 and 7 bar absolute in 0.5 bar increments were tested, measured using two Siemens Sitrans P DS III, Range: 0-500 kPa, Model number: 7MF4333-1GA02-2AB1 absolute pressure transducers. These were connected to a National Instruments 6366 USB-DAQ which sampled the pressures for 1 second during image acquisition at a rate of 1000 Hz. The mean and standard deviation of these measurements were recorded. The standard deviation of all pressure measurements was below 0.01 bar and the mean within 0.05 bar of the nominal pressure.

Bubbles were illuminated using a Constellation 120 W white 5600K LED light positioned directly behind the acrylic tank. Images were captured using a Teledyne DALSA Linea Mono linescan camera with  $8192 \times 1$  pixel resolution. The single line of pixels was sampled 10000 times at a rate of 45 kHz. These rows of pixels when stacked produced a space-time plot which was recorded on board the camera and then transmitted as a single frame to MATLAB for processing. The camera was coupled to a Questar QM100 long-range microscope using a  $1.5 \times$  Barlow lens then bellows giving a field of view of approx 900  $\mu\text{m}$  with a spatial resolution of 0.121  $\mu\text{m}/\text{pixel}$ . A schematic of the overall experimental set-up is shown in figure 1. For each condition 4 ensemble images were collected and processed separately. All data is presented as the mean of these measurements with error bars of two standard deviations applied where appropriate.

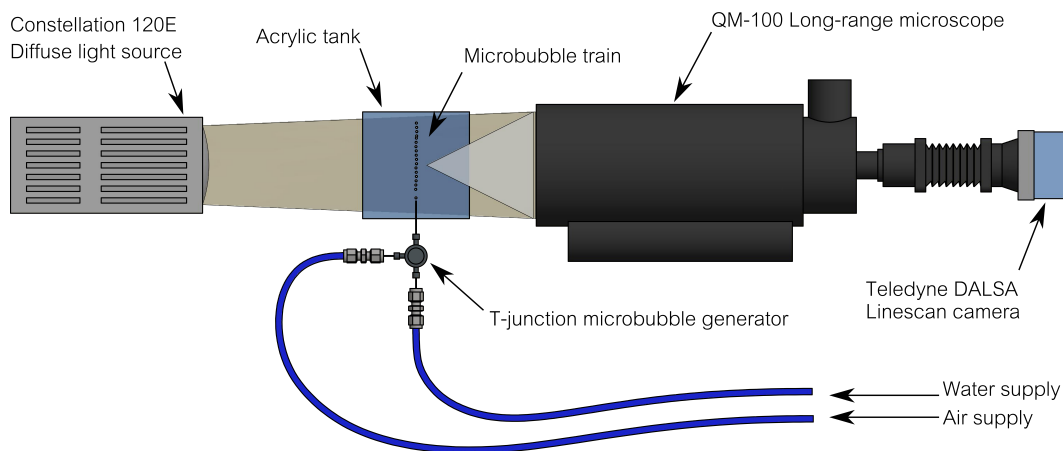


Figure 1: Schematic of experimental setup for the measurement of microbubble size and production rate using shadowgraphy

## Processing method

A small portion of an image frame is shown in figure 2. Images were acquired using the MATLAB image acquisition toolbox. Once in MATLAB each row of pixels was summed together to create a time series of integral intensity. Peaks extracted from the series correspond to the passage of a bubble through the measurement area. The single row of pixels corresponding to the maximum of each peak was extracted and the diameter of the bubble calculated via thresholding of the smoothed pixel intensity. Two methods were used to collect bubble production frequency. The first was extracted from the fast Fourier transform (FFT) of the intensity time series. In periodic production regimes this was sufficient to assess production frequency. As the device reached the limits of its operating envelope the size and frequency of the bubble produced fluctuated. The second method simply estimated the integral production frequency by dividing the number of bubbles observed in the intensity time series by the length of the sample. Comparison of this frequency estimate with the peak frequency observed in the FFT of the series allowed immediate determination of when the device was operating in its intended manner. Table 1 shows a summary of the differences between these frequencies. Large numbers signalled that the device was no longer producing mono-disperse bubbles.

Frequency Difference	$\Delta f$ (hz)	$p_{air}$ (bar)												
		1.5	2.0	2.5	3.0	3.5	4.0	4.5	5.0	5.5	6.0	6.5	7.0	
$p_{water}$ (bar)	1.5	-	-	-	-	-	-	-	-	-	-	-	-	-
	2.0	-	-	-	-	-	-	-	-	-	-	-	-	-
	2.5	-	-	-	-	-	-	-	-	-	-	-	-	-
	3.0	-	-	-	-	1	2	3	1	3	776	-	-	-
	3.5	-	-	77	1	1	0	1	1	1083	68	-	-	-
	4.0	-	-	116	2	2	1	3	2	3	378	-	-	-
	4.5	-	26	3	13	2	1	1	1	2	2	2	-	-
	5.0	-	-	-	1	0	1	3	1	373	17	594	-	-
	5.5	-	-	-	633	1	1	0	2	37	1723	1334	-	-
	6.0	-	-	-	-	-	-	1	5	15	1	21	897	-

Table 1: For each condition the table shows the absolute difference (in Hz) between two measures of the production frequency. The first measure uses the dominant bubble production frequency from largest peak in the FFT of pixel row intensity. The second measure of frequency is gathered by dividing the total number of bubbles observed over the acquisition time. Large values in this table indicates that the device was operating outside the intended principal operating mode. Conditions whose frequency measures are in agreement,  $\Delta f < 50$  Hz, have been highlighted in blue. A difference in frequency greater than 50 Hz is marked in red. A dash indicates that for this pressure combination the device either did not produce bubbles or was not tested.

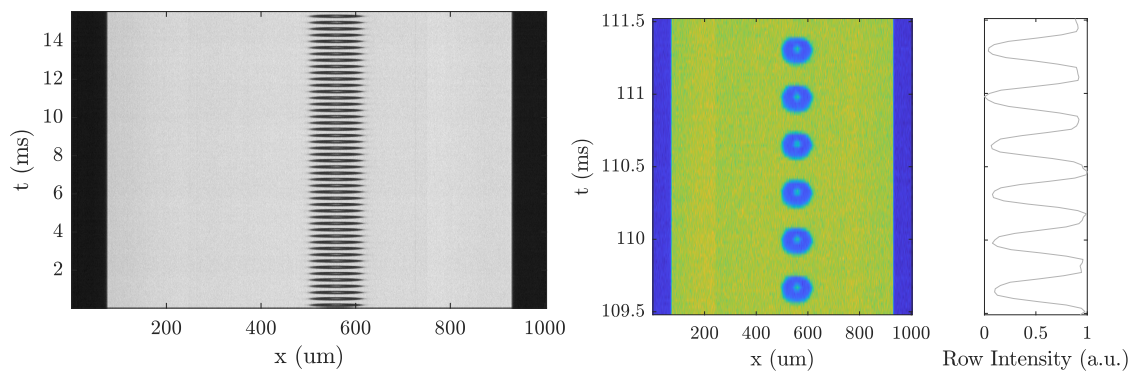


Figure 2: A sample image (left) -  $p_{air} = 5$  bar,  $p_{water} = 4.5$  bar - showing 700 lines from the line-scan camera. Here the vertical axis is time, with spatial coordinates on the horizontal axis to produce a space time plot. A portion of the regular stream of similarly sized bubbles observed in the image has been enlarged and stretched (centre). Each row of pixels in this centre image has been summed and non-dimensionalised by the minimum and maximum value of the overall series to produce the plotted row intensity time series (right). This time series is used to detect bubbles and find the centre location of each bubble for sizing.

## Results

The range of the principal operating mode can be established from examination of Table 1. For convenience the pressure ratio is defined with the air pressure as the numerator. It was observed that a pressure ratio near unity is required to remain inside the principal operating mode. The device remained stable over the largest range when an air pressure of 3-5 bar(abs) was used. At low pressure ratios there was a rapid cessation of production with the device simply ejecting water upon exceeding the critical ratio. In contrast, the breakdown of consistent production at high ratios was more subtle. The device would continue to operate but sporadically shift in and out of periodic production into a chaotic production mode. Qualitatively it was observed that this transition is often due to the disturbances created by coalescence further up in the bubble train, however this is not revealed in the data presented here.

With the conditions of interest established, the relevant data was plotted in terms of the size and frequency in figure 3. Naturally, lower air pressures produced smaller bubbles. Lower air pressures also produced bubbles at lower frequencies. As water pressure increased the bubble size reduced and the production frequency increased. This indicates bubble pinch-off occurred quicker inside the junction at these pressures. The largest bubbles of consistent size were 133  $\mu\text{m}$  in diameter, produced at an air pressure of 5 bar and water pressure of 4 bar. While the smallest bubble size was approximately 70  $\mu\text{m}$ , the two conditions where this size was observed were very close to device breakdown ( $p_{\text{Air}} = 3$  bar,  $p_{\text{water}} = 5.5$  bar &  $p_{\text{air}} = 5$  bar,  $p_{\text{water}} = 6$  bar). The smallest stable condition then was 83  $\mu\text{m}$  at an air pressure of 3 bar and water pressure of 5 bar.

Bubble production rates were of order  $10^3$  to  $10^4$  bubbles per second. In contrast to bubble diameter production frequency increased with water pressure but also with air pressure. The lowest production frequency was 770 Hz ( $p_{\text{air}} = 3$  bar,  $p_{\text{water}} = 3.5$  bar), while the highest consistent frequency was 3200 Hz ( $p_{\text{air}} = 5$  bar,  $p_{\text{water}} = 5.5$  bar). Higher, stable, mono-disperse production frequencies were achieved, but they were very close to device breakdown and could not be repeated when the combination was later re-tested. Further extreme cases were found that produced bubbles outside of these size and frequency bounds but they were either inconsistent or likely to disappear during testing.

A plane was fitted through the size data as a function of water and air pressure.

$$\text{Size}(p_{\text{air}}, p_{\text{water}}) = 110 + 13.4 p_{\text{air}} - 13.83 p_{\text{water}} \quad (\mu\text{m}) \quad (1)$$

In equation form it is clear that the mean bubble size produced was 110  $\mu\text{m}$  and that variation of water and air have similar influence but opposite effects. The size reduced or increased by approximately 13.5  $\mu\text{m}$  as the difference between these two pressures increases by 1 bar.

The adjusted R-squared residual of this fit was 0.76. Consequently approximately 24% variation in the size was left unexplained. This result is not as strong as would be desired. To improve this result, due to the speed with which measurements may be collected, electronically controlled pressure regulators could be used to conduct a more detailed sweep with increased repetition of tests. However, before testing it was assumed that the device was operating independent of its supply pressure history. Observations during testing indicate that this may not be true across short time periods at all conditions. Acquisition of samples were slowed to give time for these effects to decay - approximately 2 minutes for each pressure combination - but this effect may have contributed to errors observed here. The cause for this effect may lie in the pressure supply system. Detailed tracking of the evolving production characteristics following large pressure changes is to be conducted and compared to the supply pressure measurements in time.

## Conclusion

Bubble sizes were measured using a linescan camera to collect size and frequency measurements in near real time. Tests were carried out in quiescent water and implementation in non-stationary environments would extend the operational range. However, in this environment the principal operating mode produced microbubbles on the order of 80–130  $\mu\text{m}$  in size at frequencies ranging from 750–3200 bubbles per second were produced across the range of air and water pressures tested. Bubbles near these sizes could be used as seeded cavitation nuclei within hydrodynamic test facilities through dilute or direct injection.

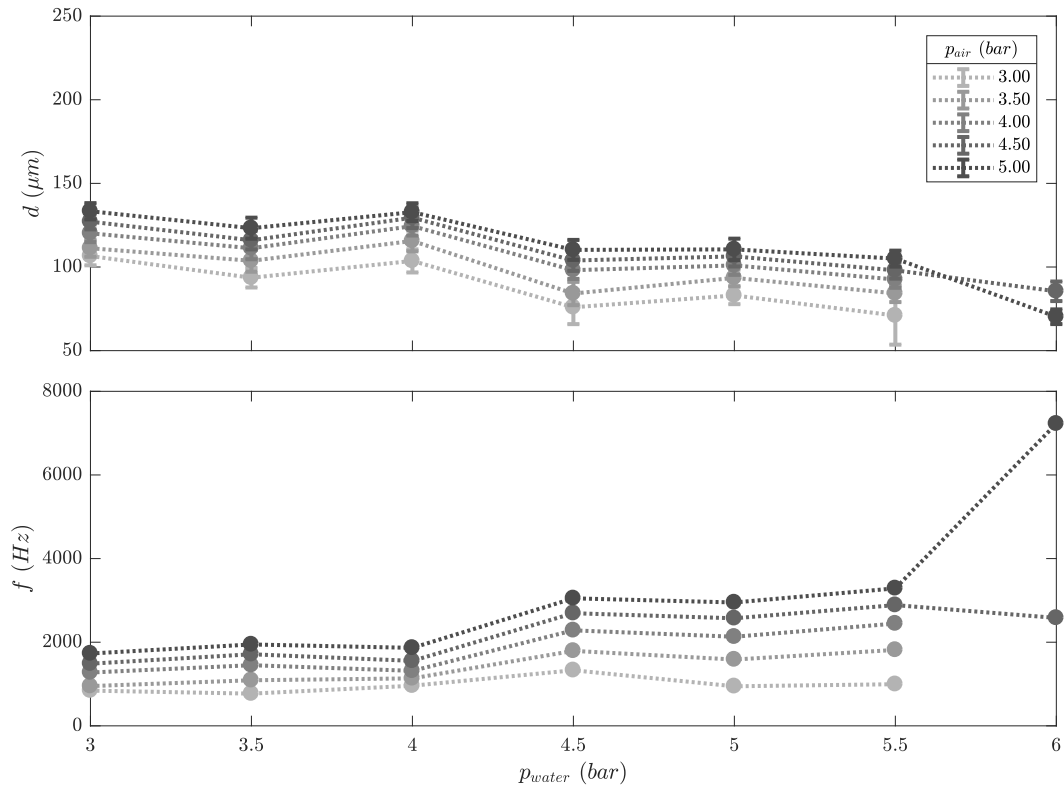


Figure 3: The diameter of bubbles produced (top) decreases as water pressure increases for a constant air supply pressure. Diameters increase with air pressure. Error bars denote two standard deviations. (bottom) Bubble production frequency increases both with air and water pressure.

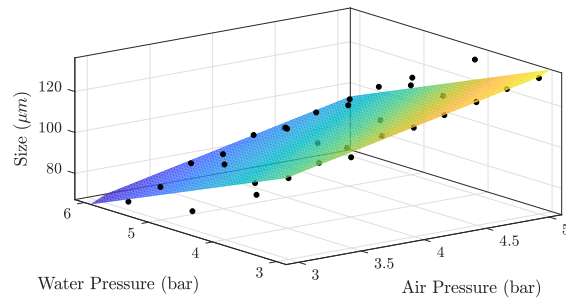


Figure 4: Size is plotted against both air and water supply pressures. A plane of best fit using least square residuals is created through the data.

## Acknowledgements:

This project was supported by the Defence Science and Technology Group (Mr. Brendon Anderson and Dr. David Clarke), the University of Tasmania, and the US Office of Naval Research (Dr. Ki-Han Kim, Program Officer) and ONR Global (Dr. Woei-Min Lin) through NICOP S&T Grant no. N62909-15-1-2019.

## References

- [1] Christopher E. Brennen. *Cavitation and bubble dynamics*. Cambridge University Press, 2013.
- [2] Jean-Pierre Franc and Jean-Marie Michel. *Fundamentals of Cavitation*. Springer Science & Business Media, 2006.
- [3] PA Brandner, Y Lecoffre, and GJ Walker. *Development of an Australian National Facility for Cavitation Research*. In Sixth International Symposium on Cavitation, 2006.
- [4] P. A. Brandner, Y. Lecoffre, and G. J. Walker. *Design Considerations in the Development of a Modern Cavitation Tunnel*. In 16th Australasian Fluid Mechanics Conference, 2007.
- [5] D Giosio, BW Pearce, and PA Brandner. Influence of pressure on microbubble production rate in a confined turbulent jet. In *20th Australasian Fluid Mechanics Conference*, 2016.
- [6] Joshua Owen, Paul Rademeyer, Daniel Chung, Qian Cheng, David Holroyd, Constantin Coussios, Peter Friend, Quentin A Pankhurst, and Eleanor Stride. *Magnetic targeting of microbubbles against physiologically relevant flow conditions*. *Interface focus*, (5), 2015.
- [7] Shelley Lynn Anna. *Droplets and Bubbles in Microfluidic Devices*. *Annual Review of Fluid Mechanics*, 48(1), 2016.